Delft University of Technology

Additional Thesis

Estimating Longitudinal River Profiles using Maximum Entropy Production

Authors:
Jeremy Trotereau, BSc (4695259)

Supervisors:
Dr. Markus Hrachowitz
Dr. Laura M. Stancanelli

April 25, 2022

Contents

1 Introduction

1.a The Maximum Entropy Production Principle

From its very inception by the German physicist Rudolph Clausius, the concept of entropy was defined as one that is maximised. This fact is nowadays known as the Second Fundamental Law of Thermodynamics. This gives an accurate representation for isolated systems in equilibrium (Koutsoyiannis, 2014). However, the earth system is one that is constantly fed energy by the sun, and therefore never reaches thermodynamic equilibrium. In figure 1, we can see the way that the earth is irradiated by the sun, and re-emits radiation into outer space (Kleidon, 2020).

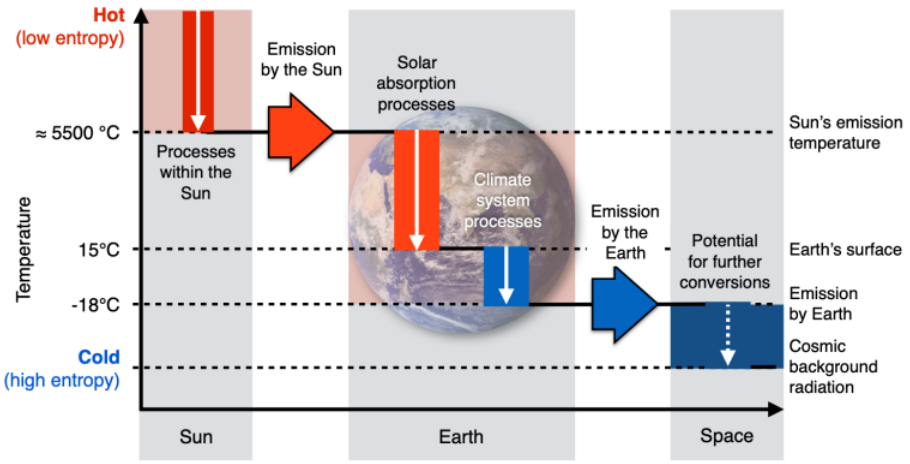

Figure 1: A schematic representation of the entropy degradation of solar radiation by the earth system, from Kleidon (2020).

These transient systems do, of course, obey the conservation laws of mass, momentum and energy. However they generally have more degrees of freedom than can be fixed by these three laws. The question faced by scientist in the mid 20th century is therefore the following: When choosing from a multitude of different system outcomes, all of which obey the conservation laws, which one does Nature choose?

A number of principles were found by scientists across many different fields which gave positive outcomes, such as Prigogine's principle of minimum entropy, exergy, maximum power, depletion of gradients (Kleidon et al., 2010). However, in this paper we will focus on Maximum Entropy Production Law (usually Principle is preferred) as proposed by Swenson (1997). This is a much stronger statement than that of Clausius, which merely shows that entropy increases.

The Maximum Entropy Production Principle (MEPP) states that when a system is far from thermodynamic equilibrium, it will tend to maximise the production rate of entropy. Swenson (1997) originally used it in Biology, but it has since then been used in hydrology (Maheu et al. (2019), Kleidon et al. (2010), Kleidon et al. (2006), Porada et al. (2011), Zhao et al. (2016)). Though not always successfully (Westhoff and Zehe, 2013).

1.b River morphology

In this report, we examine the applicability of the MEPP on the shape longitudinal profile of river. This too has been the object of extensive research in the past. Attempts include using functions such as exponentials (Yatsu, 1955), power laws (Osterkamp et al., 1983) or cycloids (Saville, 2013) which often contain break points, or the use of thresholds (Chang, 2008).

To examine the applicability of the MEPP on longitudinal river morphology, we will derive a theoretical shape and perform a validation. We strive to answer the questions: Which shape would a river following the MEPP have, and is this shape consistent with observations?

2 Derivation

2.a Notes on the sources

The goal of this derivation will be to derive a curve which maximises entropy production. This derivation is based on a similar derivation by Jenkins and Inman (2006). It should be noted that this paper has been criticised by Maldonado and Uchasara (2019). Their critique on the validity of the derivation is based on the fact that other curves can be found that create more entropy than the curve derived by Jenkins and Inman (2006).

Though this is true, fitting a curve such (such as a straight line) through the equilibrium beach profile is likely a breach of the restrictions mentioned in the paper by Martyushev and Seleznev (2013). More specifically, the Local Equilibrium Hypothesis would be broken, due to the excessive erosion of sand near the bottom. In fact, it is hard to argue at all that a straight line constitutes an *equilibrium* beach profile.

It should also be noted that a very similar derivation was performed for the transverse profile of glacial valleys by Hirano and Aniya (1988) and improved by Morgan (2005) and Faraoni (2020).

2.b Thermodynamics

The goal of this derivation is to find the curve $x = \zeta(z)$, where z is the elevation of the river surface, and x is the longitudinal upstream coordinate. This means that $x = 0$ is situated at the mouth and $x = x_{max}$ is situated at the top of the river. For our purposes, this "top" is arbitrary point along the river. And it means that $z[x = 0]$ is at the height of the mouth of the river. This is not necessarily at sea level, as some rivers we looked into were endorheic, and others were tributaries to larger rivers.

We start by defining the derivative of our unknown curve:

$$d\zeta = \sqrt{(dx)^2 + (dz)^2} = \sqrt{1 + x'^2}dz \tag{1}$$

Where $x' = \frac{dx}{dz}$. And its reciprocal, $z' = \frac{dz}{dx}$.

We then continue by drawing a free-body diagram around the area of interest, which in our case would be a river. Jenkins and Inman (2006) then calculate the system's contribution to the total entropy in the universe.

$$\frac{\partial S}{\partial t}_{Universe} = \int_V \frac{\Phi}{T_a} dV = \frac{P_{diss}}{T_a} \tag{2}$$

Where Φ is the average rate of dissipation of mechanical energy per unit volume. Also known more simply as the "entropy production density". P_{diss} is the total energy dissipation rate. T_a is the temperature.

The dissipation of energy can be derived using work:

$$P_{diss} = 2 \int_{\Delta t} F_{fric} du \tag{3}$$

Where F is the friction force causing energy dissipation.

In our case, the friction forces come mostly from turbulent viscosity, which is often modelled as a viscous friction. A viscous shear force is modelled as: $\tau = \mu \frac{\partial u}{\partial x}$ where x is an arbitrary spatial direction. In this derivation, we assume that cross-river velocity gradients are negligible, and the same goes for long-river gradients.

For the power per horizontal area of river , we integrate over the water depth.
This gives:

$$\frac{dP_{diss}}{dA} = \int\int 2\mu \frac{\partial u}{\partial h} dh du = \mu u^2 \tag{4}$$

Now we have already assumed that the cross-river profile is approximately constant, so we can split out the river width and integrate over the length of the river.

$$P_{diss} = W \int \mu u^2 d\zeta \tag{5}$$

Filling this into equation 2, this gives:

$$\frac{\partial S}{\partial t}_{Universe} = W \int \frac{\mu u^2}{T_a} d\zeta \tag{6}$$

2.c Fluid mechanics

We have to find a set of equations that describe the average stream velocity. A simple example is the Chézy formula.

$$u = C\sqrt{Ri} = C\sqrt{Rz'} \approx C\sqrt{dz'} \tag{7}$$

Where C is the Chézy coefficient, R is the hydraulic radius and i is the river's channel slope.
For wide rivers, we can assume that the hydraulic radius R is approximately equal to the depth, which is also a function of the channel slope.

$$d = \left(\frac{q^2}{C^2 i}\right)^{1/3} = \left(\frac{q^2}{C^2 z'}\right)^{1/3} \tag{8}$$

Combining equations 7 and 8, and assuming that the rivers we analyse have constant width, this gives:

$$u = C^{2/3} q^{1/3} (z')^{1/3} = \frac{C^{2/3} Q^{1/3} (z')^{1/3}}{W^{1/3}} \tag{9}$$

For this derivation, we assume that temperature is only weakly linked to height, and we therefore assume uniform temperature.
This means that we can extract the temperature from the integral giving:

$$\frac{\partial S}{\partial t}_{Universe} = \frac{W^{1/3}\mu}{T_a} \int C^{4/3} Q^{2/3} (z')^{2/3} d\zeta \tag{10}$$

2.d Euler-Lagrange Maximisation

Jenkins and Inman (2006) then use the Euler-Lagrange formula to maximise the entropy production, and so will we.

$$F(x, x', z) = C^{4/3} Q(z)^{2/3} z'^{2/3} \frac{d\zeta}{dz} = C^{4/3} Q(z)^{2/3} z'^{2/3} \sqrt{1 + x'^2} \tag{11}$$

We clean up by defining $A = C^{4/3} Q(z)^{2/3}$.
Using the Euler-Lagrange equation such as used by Jenkins and Inman (2006), Hirano and Aniya (1988) and Faraoni (2020):

$$\frac{d}{dz}\frac{\partial F}{\partial x'} - \frac{\partial F}{\partial x} = 0 \tag{12}$$

Combining equations 11 and 12, and using the fact that $\frac{\partial F}{\partial x} = 0$, we obtain.

$$\frac{d}{dz}\frac{\partial}{\partial x'}\left[Az'^{2/3}\sqrt{1+(x')^2}\right] = 0 \tag{13}$$

Before calculating the derivative, we use the fact that $x' = (z')^{-1}$.

$$\frac{d}{dz}\frac{\partial}{\partial x'}\left[\frac{A}{(x')^{2/3}}\sqrt{1+(x')^2}\right] = 0 \tag{14}$$

We integrate the right-hand side, which gives:

$$\frac{\partial}{\partial x'}\left[\frac{A}{(x')^{2/3}}\sqrt{1+(x')^2}\right] = B \tag{15}$$

Next, we calculate the derivative with respect to x', which gives the expression below.

$$\frac{x'^2-2}{3x'^{5/3}\sqrt{1+x'^2}} = \frac{B}{C^{4/3}Q(z)^{2/3}} \tag{16}$$

We simplify the function by writing:

$$f(x') = \frac{x'^2-2}{3x'^{5/3}\sqrt{1+x'^2}} \tag{17}$$

$$g(z) = \frac{B}{A} = \frac{B}{C^{4/3}Q(z)^{2/3}} \tag{18}$$

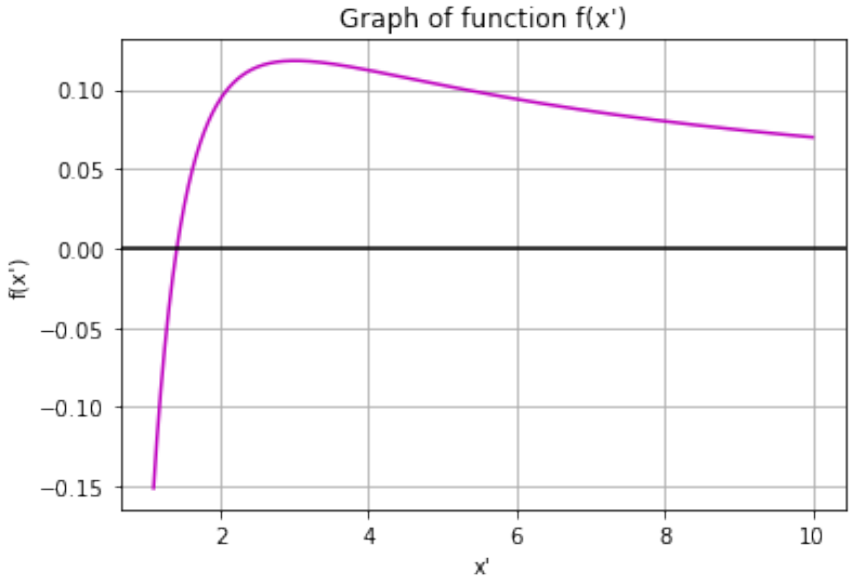

Figure 2: Graph of $f(x')$ as defined in equation 17

2.e Numerical implementation

Starting from the equality $f(x') = g(z)$, we use the Newton-Raphson method by subtracting $g(z)$ from both sides ($f(x') - g(z) = 0$), and then finding the roots. Doing this for many points gives a new function. For an infinite set of points this would be equivalent to finding the inverse of $f(x')$

$$x' = \frac{dx}{dz} = f^{-1}(g(z)) \tag{19}$$

In practice, the nature of $f(x')$ does not make it invertible for all values of g(z). This is because the range of $f(x')$ is $(-\infty, 0.118)$ as can be seen in figure 2. Because the Newton-Raphson method is locally convergent, and we focus on values above 3.5, the domain of the inverted function is in fact only $(0, 0.118)$. In our code, the domain is limited further to $(0.005, 0.118)$ to avoid very large values of x'. The maximum value is $x'_{max} = f^{-1}(0.005) \approx 544.32$.

To ensure that equation 16 can be inverted, the integration constant B in $g(z)$ (see equation 18) is set such that the maximum and minimum values of $g(z)$ fit within the domain. When that is not possible, range of z is restricted.

The last step is to integrate both sides to obtain x.

$$x = \int_0^x dx = \int_{z_{min}}^{z} f^{-1}(g(z))dz \tag{20}$$

The resulting curve will be referred to as the "MEPP curve". It should be noted that the integration with respect to z is unusual and it is perhaps a little confusing to see when plotted (for instance, a constant line is vertical).

3 Validation

The derived function was programmed in python. As discussed above, the function is the numerically inverted and integrated to obtain the predicted longitudinal coordinates as a function of height, using discharge as an input.

3.a Validation data

The discharge data was provided as daily time series for different stations by the Global Runoff Data Centre GRDC by Looser et al. (2020). Stations have given spatial coordinates, and some stations also have a given elevation. Gaps in this data are filled using the Digital Elevation Model (DEM). It is worth noting that by using the station discharge data (which typically have a length of 20 years) and assuming that the values represent a stationary river, that we assume that the river relaxation time is (much) shorter than the length of the discharge data. This is possibly problematic for low-discharge rivers.

Two methods of converting the time series into a stationary data were applied, each supporting a different hypothesis about how river morphology changes. The first method is to take the mean water discharge ($\overline{Q}$), which implicitly assumes that the river morphology is most strongly affected by the mean flow. The second method is to take the mean annual peak flow (Q_{max}), which implicitly assumes that annual peak flows show have a larger contribution on river morphology. These two were chosen because in field observations, Bertoldi (2010) find that both have effect.

The simple logarithmic model $Q(z) = \ln(z/a)/b$ (where a and b are fitted constants) was used to fit both data, as a first order approximation. The fitting was performed using a Weighted Least Squares Estimation (WLSE), where weighting was a function of the product of the catchment upstream area and the length of the data in years. The exact function is given in equation 21. This is done because a larger upstream catchment area gives a smoother outflow, and because the number of years in the data is a good proxy for the variance of the flow (if we assume that the mean and max flows are independent from year to year).

$$W_{WLSE} = \frac{1}{\sqrt{A_{\text{upstream}} N}} \tag{21}$$

Where A is the catchment upstream area and N is the number of years in the time series.

In figure 3, the $\overline{Q}$-z diagram is shown, with the two types of stations, as well as the fitted log function $\overline{Q}(z)$.

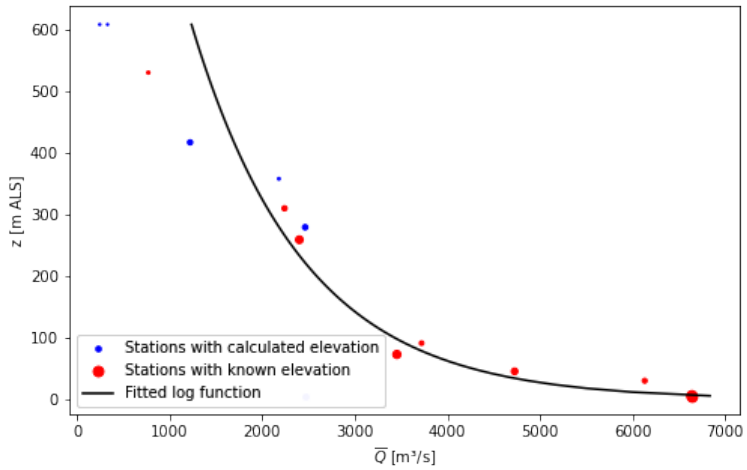

Figure 3: $\overline{Q}$-z diagram for the Yukon river in Alaska, with stations with given (calculated) height in red (blue), and the WLSE fitted log function in black. The area of the circles corresponds with their weight in fitting.

As can be seen from figure 3, we assume the discharge to be monotonically decreasing as the elevation z increases. Furthermore, we can see that in this particular instance, the fitted function gives a good representation of for the stations below 400 meters. Above that, the fit deviates from the points, at least in part because of the weighting system we utilized.

For the validation data, topographical river locations were combined with a Digital Elevation Model (DEM) to calculate the river heights. The river locations were provided by HydroSheds (Lehner et al., 2008). The DEM used below 60 degrees of latitude was GTOPO30 DEM, courtesy of the U.S. Geological Survey (USGS, 1996). Above 60 degrees, the ArcticDEM courtesy of the Polar Geospatial Centre (PGC) (Porter, 2018) was used. The DEM was sampled at points along the river locations in order to find longitudinal elevations.

In figure 4, the rivers studied in this research are highlighted in blue. These are overlayed on a map of the world's coatlines (in brown) for geographic reference. Major studied rivers include the Mississippi river basin and the Niger. Note that the Saskatchewan river in the Canadian Arctic is a tributary of the Nelson river (with a lake in between).

To be chosen, rivers had to fit two criteria.

1. They have to be long enough to allow for many points to be taken from the DEM, increasing precision.

2. They have to have many discharge-measuring stations (at the very least 2) along the course of the river, with long time series.

For the project, an important tertiary concern the quantity of engineering performed on the river. As stated in Ylla Arbós et al. (2021), only a third of major global have not been subject to

major engineering. This is problematic, because engineered rivers break a number of assumptions made in the derivation. Notably, they are not in steady state, vary wildly in width, and most likely do not maximise entropy in their current state.

This third criterion was often broken, however, to test the limits of the MEPP derivation.

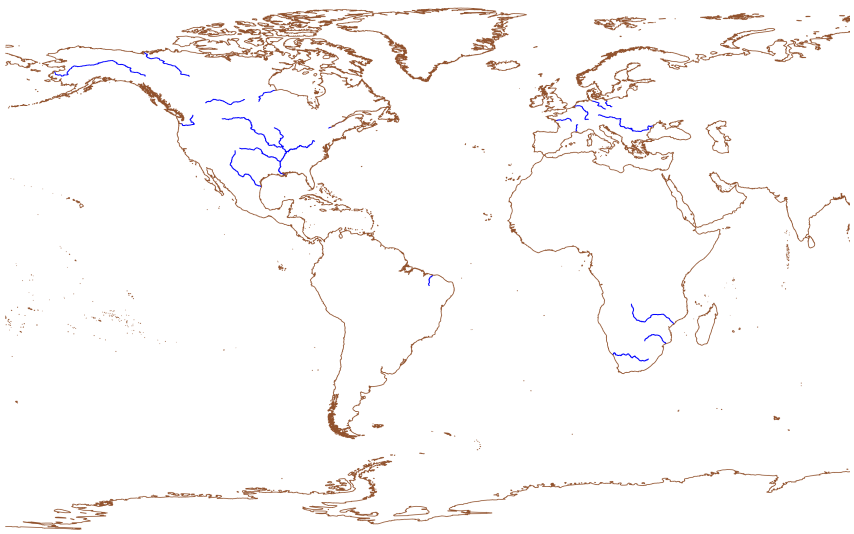

Figure 4: Map of analysed rivers (in blue). An exhaustive list of rivers used in this project and important data concerning those rivers can be found in the Appendix

The values of the longitudinal elevations are smoothed using a rolling quantile function, called *qsmooth*. The window width is set to one-fiftieth of the data, so 2%, and the quantile to the lowest 5th percentile. These values are somewhat arbitrary, but prove to give good results. The advantage of these values is they select the lower points (where the river would logically be) however, this does induce a bias in the data.

In figure 5, the effect of the smoothing function is shown.

Finally, x coordinates of the river are calculated. This is done using the final formula as found in equation 20. $x(z, Q(z), B, C)$, is given the smoothed height values z, the fitted logarithmic function $Q(z)$ and a Chézy constant value of 43, based on an interpolation of the values for "Straight stable deep natural channel" (C = 49) and "Variable rivers, vegetated banks" (C = 37) from table 2 in Warmink et al. (2007).

The resulting curve can then be compared with the data. An example of the two overlayed can be found in figure 6. To quantify the goodness of fit, the Mean Absolute Bias (MAB, see equation 22) was calculated for each river for both the mean water discharge and mean annual peak flow discharge types.

$$MAB = \frac{1}{N} \sum_{j=0}^{j=N} |x_j - x(z_j, Q(z_j), B, C)| \tag{22}$$

Where N is the number of points (x, z) in the validation data.

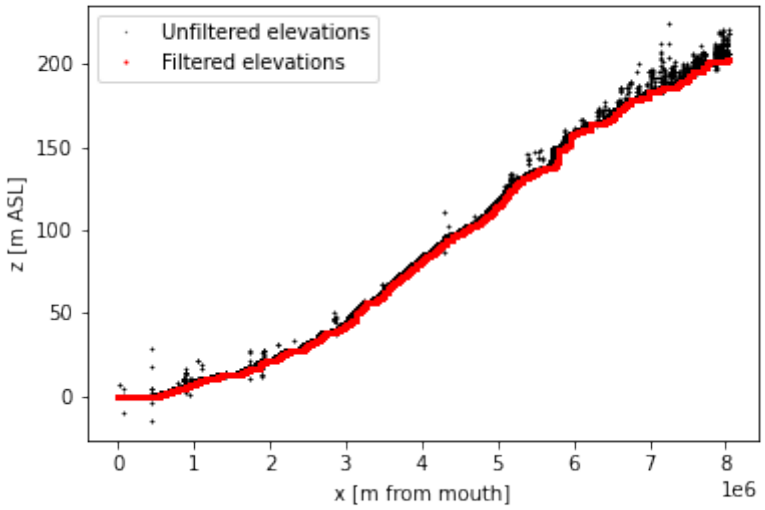

Figure 5: Observed longitudinal river profile for the Mississippi river before (after) using quantile smoothing in black (red)

For the final analysis, we use normalised data according to the following equations, with the additional constraint that all values of x and z must be positive.

$$x^\star = \frac{x - x_{min}}{x_{min} - x_{max}} \tag{23}$$

$$z^\star = \frac{z}{z_{max}} \tag{24}$$

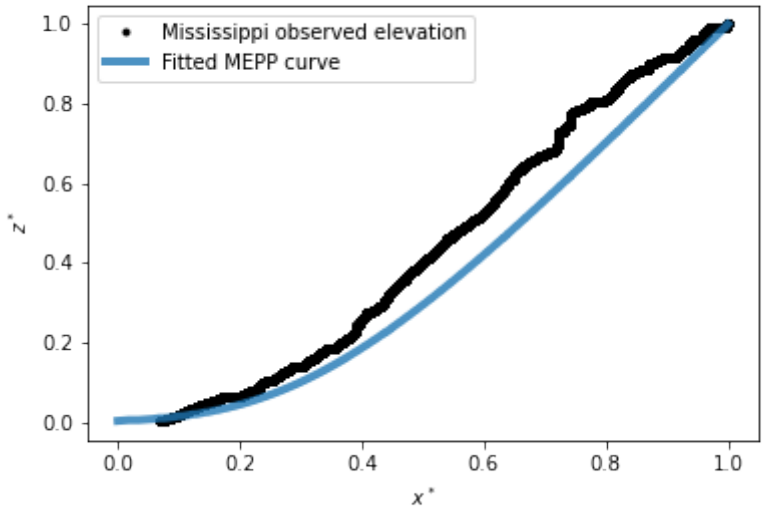

Figure 6: Smoothed observed longitudinal river profile of the Mississippi river (in black) compared with fitted MEPP function (in blue). Both axes are normalised according to equations 23 and 24.

4 Results & Discussion

An overview of the results can be found in figure 7. It should be noted that the results and all other data showed are also tabulated in the Appendix.

The MAB (Mean Absolute Bias) is calculated from normalised data, so the values are relatively small. As the x (remember we calculate the MAB and RMSE using the x coordinates) values are bound between 0 and 1, the MAB is also. The MAB was chosen for its ease of interpretation as it effectively measures the area between the two curves. (It is not that simple, as the points are not evenly spaced, but it is a reasonable approximation). This approximation has the practical advantage that the "area between the curves" is independent of viewing direction.

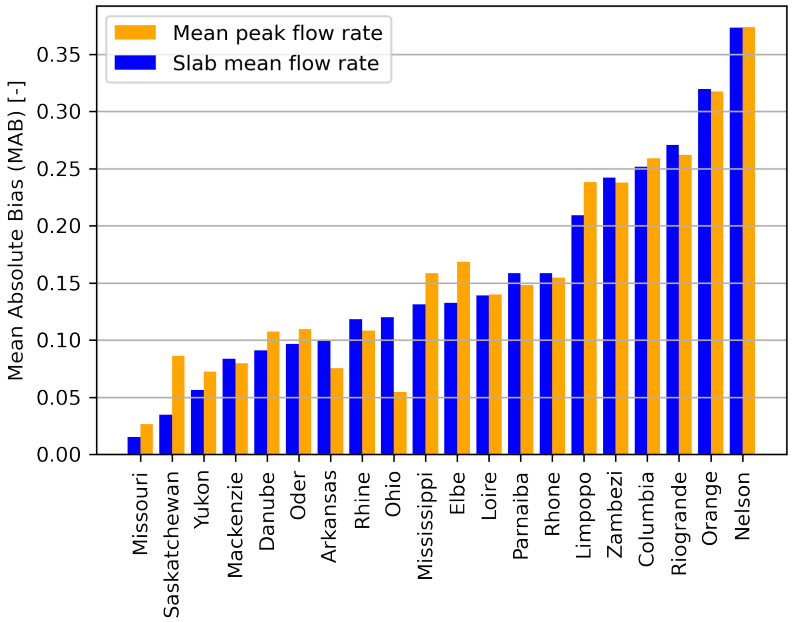

Figure 7: MAB of the results sorted by MAB from the mean discharge

Looking at figure 7, we can see that there is a large variation between the MABs of the different rivers. Indeed, we can see that the Missouri performed an order of magnitude better than the Nelson river.

From figure 7, we do not see any particular pattern. We do not see a strong difference in performance between the mean and peak flow rate, nor do we see any geographic pattern in the location of the rivers. For instance, the Saskatchewan is a tributary of the Nelson, so we would expect similar results, but this is clearly not the case.

We do see that in individual cases, the mean discharge or mean annual peak flow rate strongly outperforms the other, such as the Saskatchewan or the Ohio rivers. This is due to a significant change in the logarithmic fit for the discharge-height relationship. Generally, changes in scale are compensated by the integration constant B. Changes in the shape of the logarithmic fit due to changes in input can cause strong variations in results.

In figure 8, we checked using linear regression whether the length of the river, the mean slope, the mean or maximum discharge, the number of discharge stations and the MAB of the logarithmic

fit of Q are good predictors of the MAB of the MEPP curve for the mean water discharge.

Figures of possible correlations

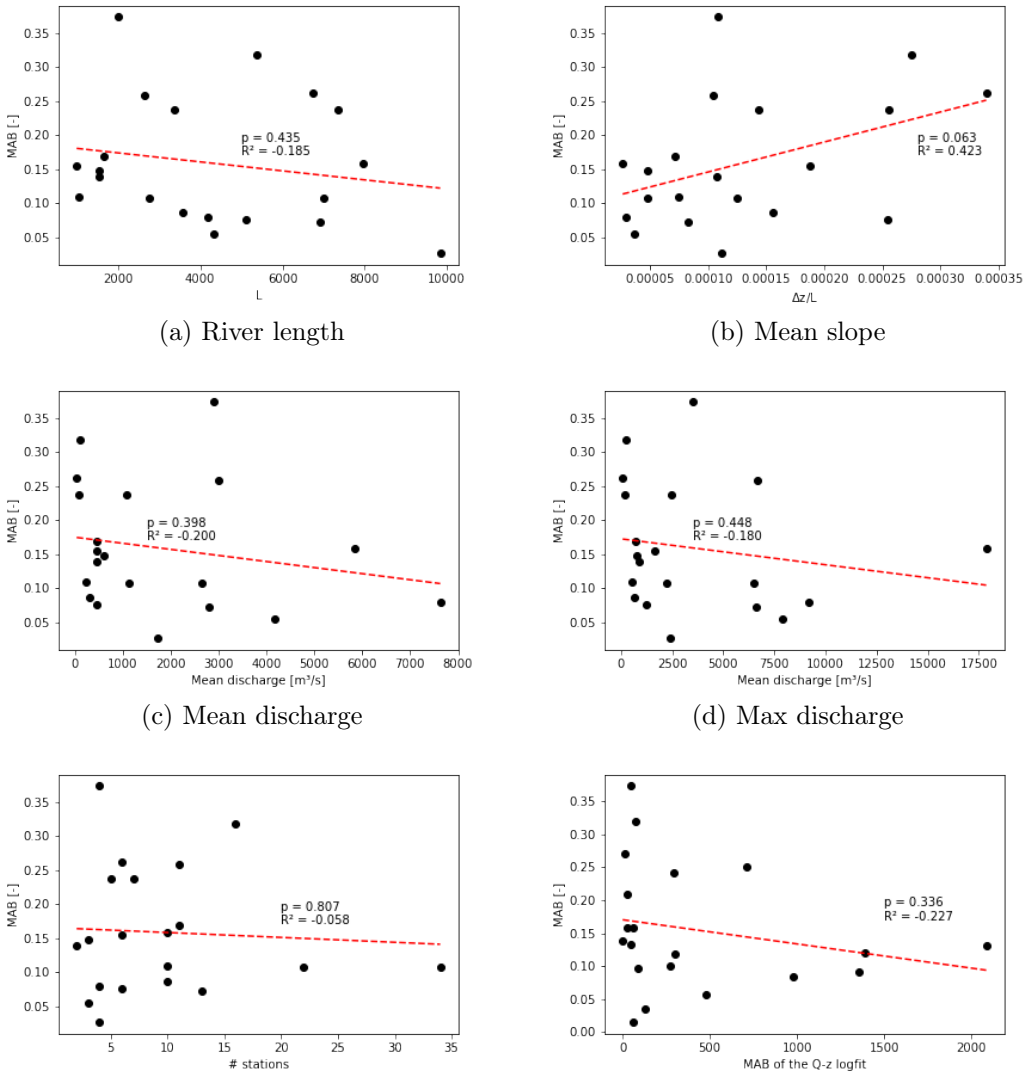

(a) River length

(b) Mean slope

(c) Mean discharge

(d) Max discharge

(e) Number of discharge stations

(f) The MAB of the log fit parameters

Figure 8: Analysis of possible correlations between river properties and the MEPP goodness-of-fit (MAB)

Looking at figure 8, we can state that only one of the aforementioned factors might be good predictors of the MAB. This has a number of implications, which we will discuss one by one below.

The fact that there is no clear link between river length (fig. 8a) and RMSE implies that the DEM had a relatively small impact on the results. If there had been a strong link between river length and MAB, then this might have to do with the coarseness of DEM, which affects small objects

more than large ones. But as this does not happens, we can reject this hypothesis. Importantly, we conclude from this that the DEM employed can support the analysis of smaller watercourses.

The only possibly good predictor is slope (fig. 8b). More specifically, it seems that steeper rivers have higher MABs. This can be debated on the basis of our small sample size (about 20 rivers) and the poor p-value and correlation coefficient. However assuming, for now, that this relationship is true, we would explain it it two ways: The first is by pointing out that steeper rivers might break some hypotheses, notably the hypothesis on constant river width. The second is that steeper rivers are more inviting for placing dams, which, as we will see, significantly increases their MAB. Both of these hypotheses also help explain the low correlation coefficient. There is no law of nature dictating the placement of dams, nor are there clear patterns (other than a gradual widening over long distances) in river width. This variability is reflected in the the variable MAB.

There is also no clear link between either mean or maximum discharge and MAB (fig. 8c and d). This is against our expectations, as a smaller (peak) discharge would likely have a smaller sediment discharge, which implies a longer relaxation time. Therefore, one would expect a lower MAB for larger discharges. As this is not the case, we can assume that the dryer watercourses were generally no less in equilibrium than the curves with higher (maximum) discharges.

Interestingly, there is no clear link between having more station data and having a lower MAB. This likely has to do with the logarithmic fit we performed. Taking the example of the Danube, with 34 stations along the river, in figure 9.

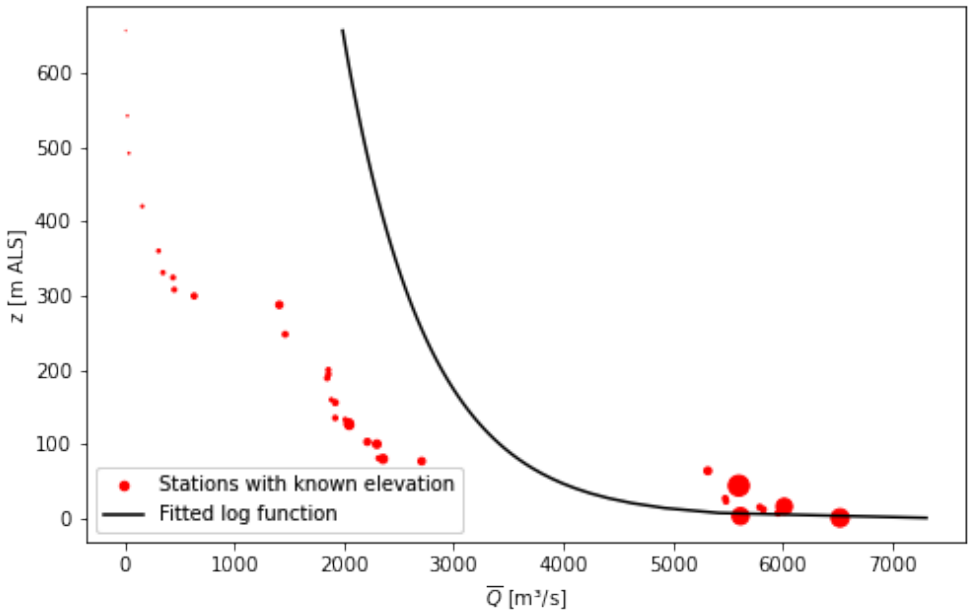

Figure 9: Logarithmic fit using Weighted Least Squares Estimation on Danube discharge data

In figure 9, we see that the logarithmic curve does not properly follow the data, mostly as a consequence of the weighting system. This means that adding more points especially in the higher reaches of the river, contributes very little to improving the accuracy of the model.

Finally, there is no clear correlation between the MAB of the MEPP curve and that of the logarithmic Q(z) profile (fig. 8f). This is remarkable, as one would expect that a poor Q-z would automatically lead to the poor performance of a river. But as we hinted at when talking about slope, the influence of dams does disrupt the data.

To generalise what we discussed above, from figure 8, we can state that in general, it is unclear which effects have an impact on the goodness-of-fit of the MEPP curve. This, of course, requires a more thorough quantitative analysis, using more rivers. But more importantly, it is also a demonstration of the limitations of the derived curve, which shows significant variability when tested on different rivers. In short: the results show that the derived curve is far from perfect. This means that for now, this method will have to be used as a first-order approximation of longitudinal river morphology.

Moving away from the quantitative analysis, we can also find two important qualitative reasons that explain some high MAB values: tributaries and dams.

Returning to figure 9, we can see two discontinuous jumps at elevations of about 50, 250 and 300 meters. These are where the Tisza and Sava, Drava, and Iller and Inn rivers respectively have confluences with the Danube. These tributaries create considerable discontinuities within the the discharge-elevation graph, which are not captured by the logarithmic fit.

To find a good example of the effect of tributaries on the morphology of a river, we will consider the example of the Rio Grande (see fig. 10). The first notable observation is the poor fit of the curve in figure 10b, which, as it can be seen, corresponds with a very poor fit of the logarithmic discharge model in figure 10a. The second and more important point is that in figure 10b, at an upstream distance of about 0.6, there is a break point in the curve. In reality, this break point coincides with a confluence between the Rio Grande and Rio Conchos, which is its largest tributary Garrick (2018).

Results for the Rio Grande river

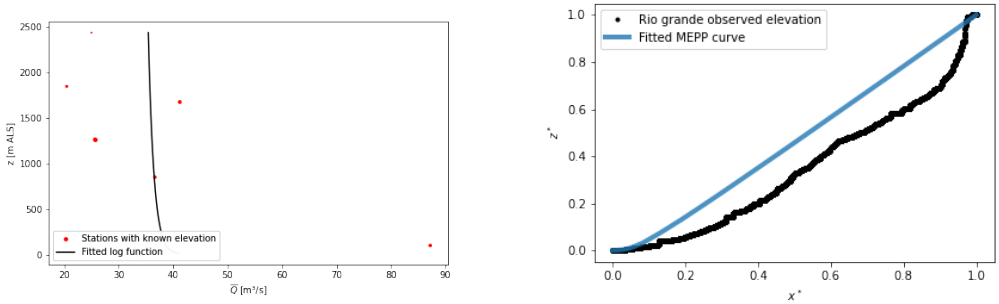

(a) Q-z diagram (b) Fitted MEPP curve

Figure 10: Results for the Rio Grande river. On the left the relatively poor Q-z plot. On the right the resulting poor fitted MEPP curve. Note that as Q(z) is almost constant, the MEPP curve, which is an integral with Q(z) as on of its arguments, is almost a straight line.

Dams also have a large impact on the MAB. To explain this, we should remember that the DEM that was used does not measure bathymetry, but water surface. This effectively means that the assumption that we made about the difference between river bed elevation and river surface elevation being negligible does no longer hold. The same goes for an assumption of constant width. Furthermore, dams filter sediment from water, severely impacting the way the river erodes. This also means that a river with recent dam engineering work are also not in equilibrium.

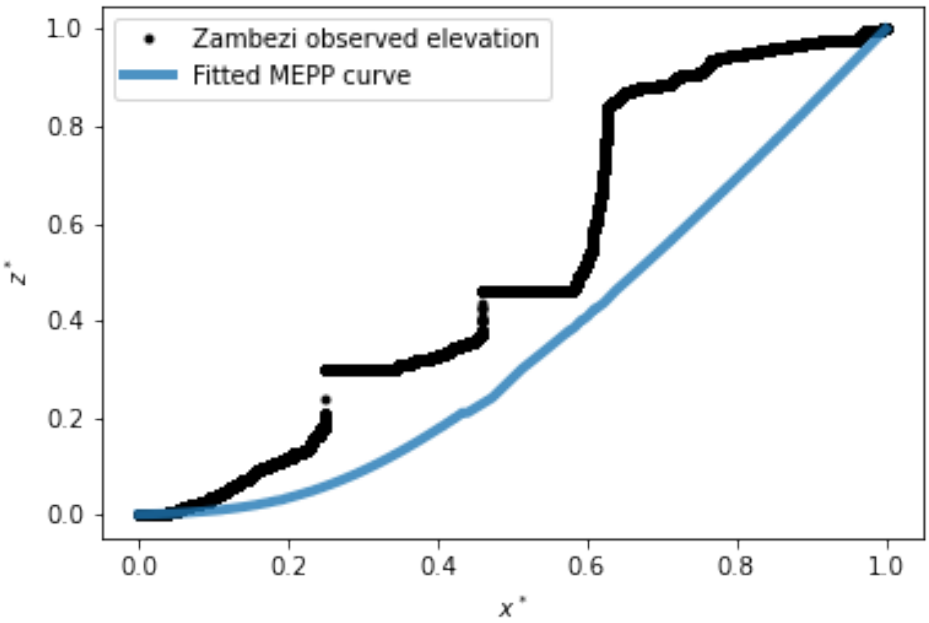

Figure 11: MEPP curve and validation data for the Zambezi river

The Zambezi river is an excellent example of how dams are poorly modelled by the derived MEPP curve. As can be seen in figure 11, the Zambezi water surface has a shape that strongly differs from that predicted by the MEPP curve. Furthermore, we can also clearly see the placements of the dams in the observed elevation at upstream coordinates 0.2, 0.45 and 0.6.

However, a word of caution must be said before generalising that "all antropogenic riverine disruptions yield poor MABs". The Missouri, Rhine and Danube performed well in our analysis despite labelled "examples of [...] heavily engineered rivers" by Ylla Arbós et al. (2021). The difference between the engineering mentioned by Ylla Arbós et al. (2021), which is mostly to improve navigability and the dams we referred to above is the scale of the disruption. We therefore postulate that the scale of engineering is a better predictor of poor MEPP performance than the "naturalness" of a river. This is unsurprising as small changes to the river do not significantly impact the river elevation, therefore having little impact on the goodness of fit.

Conversely, this means that the MEPP curve also performs well on rivers engineered for navigation, meaning that it can also be applied on the many larger rivers that do have major engineering performed to them.

5 Conclusion & Recommendations

In this report, we have described the following results:

Firstly we have shown that it is indeed possible to derive an idealised river profile using the Maximum Entropy Production Principle (MEPP). Though by no means an elegant expression, it is simple in the way that this curve is dependant only on discharge values in the river. We have managed to find a numerical solution to the derived equation and have managed to apply it to 20 rivers.

Secondly we have attempted to validate this curve, with mixed results. Using the Mean Absolute Bias (MAB) as an objective function, we see an order of magnitude of difference between the best- and worst performing rivers.

Finally, through qualitative and quantitative analysis, we have found that the presence of large dams and the average steepness of rivers are two likely influences on the goodness-of-fit of the derived MEPP. The presence of dams dramatically changes the longitudinal elevation profile, in a way that Nature does not perform. As a result, performance suffers. Steeper rivers perform more poorly, possibly because they are more likely to contain dams, but equally possibly because might break some assumptions, such as the presence of a homogeneous cross section.

For future research, we suggest two paths. One testing and extending the applicability of the MEPP curve in the field of geomorphology. Questions that remain unanswered include:

1. What can be said about the influences of various river parameters (e.g. those chosen for figure 8) when more rivers are analysed?
2. In our analysis we used mean and annual max flows. Which quantile is the best representation?
3. Does the MEPP curve also hold on smaller watercourses?
4. Does the MEPP curve also hold for watercourses created under laboratory conditions?
5. Does the MEPP curve also hold for subsections of rivers, where the start or end of such a subsection is a dam?
6. Does the MEPP curve also hold for intermittent watercourses?
7. What timescale is the relaxation time?
8. Can we find a better curve than logarithmic for the Q-z diagrams?
9. Can we include the discontinuities caused by tributaries in our Q-z diagrams?
10. Can this approach be extrapolated into the field of glaciology (using assumptions similar to the glaciologist Faraoni (2020))

The second is to test if the equations derived could also be used as a remote sensing tool. As there is a one-to-one relationship between the discharge and the river gradient (which we use, see equation 16), the reverse is also true. Would it be possible to use the shape of the river to estimate its (mean) flow characteristics?

6 Appendix

6.a Appendix I: River information

Name -	Length [km]	Δz [m]	# Points -	# Stations -	Lowest $\overline{Q}$ [m^3/s]	Average $\overline{Q}$ [m^3/s]	Maximum $\overline{Q}$ [m^3/s]
Amazon	14574	484	48250	6	47101	116245	169490
Arkansas	5117	1304	20068	6	15	450	1266
Columbia	2640	274	10745	11	10	3013	6684
Danube	6991	331	289977	34	13	2653	6527
Elbe	1660	119	76527	11	288	461	694
Limpopo	3373	862	119072	7	21	93	183
Loire	1532	164	64926	2	3	457	912
Mackenzie	4170	122	22727	4	4926	7628	9197
Mississippi	7962	209	30002	10	84	5840	17861
Missouri	9836	1095	41497	4	1129	1732	2385
Nelson	2008	217	9386	4	2224	2913	3540
Oder	1039	77	46454	10	42	222	514
Ohio	4329	159	16704	3	1190	4180	7908
Orange	5381	1479	198869	16	18	115	252
Parana	7173	322	24791	5	1551	13865	17764
Parnaiba	1544	74	2683	3	427	618	768
Rhine	2750	343	116244	22	117	1127	2246
Rhone	989	186	37351	6	3	461	1653
Rio grande	6725	2284	24681	6	20	39	87
Saskatchewan	3571	557	16972	10	54	298	684
Yukon	6926	573	4441	13	246	2809	6640
Zambezi	7354	1056	247492	5	11	1087	2463

Table 1

6.b Appendix II: MAB values

River	MAB using $\overline{Q}$	MAB using Q_{max}	MAB_{Q-z} using $\overline{Q}$	MAB_{Q-z} using Q_{max}
Arkansas	1.0001e-01	7.5163e-02	2.7311e+02	1.0964e+03
Columbia	2.5160e-01	2.5688e-01	7.0883e+02	2.5705e+03
Danube	9.1031e-02	1.0759e-01	1.3545e+03	2.2799e+03
Elbe	1.3248e-01	1.6836e-01	4.8345e+01	1.5997e+02
Limpopo	2.0929e-01	2.3833e-01	2.7117e+01	4.2903e+02
Loire	1.3888e-01	1.3984e-01	6.0840e-14	2.4869e-13
Mackenzie	8.3545e-02	7.9851e-02	9.7659e+02	3.2610e+03
Mississippi	1.3103e-01	1.5869e-01	2.0845e+03	6.2574e+03
Missouri	1.5097e-02	2.6591e-02	5.9043e+01	1.4917e+02
Nelson	3.7328e-01	3.7367e-01	4.4346e+01	5.2653e+01
Oder	9.6727e-02	1.0961e-01	8.7156e+01	1.8683e+02
Ohio	1.2004e-01	5.4631e-02	1.3918e+03	2.5195e+03
Orange	3.1938e-01	3.1739e-01	7.0552e+01	5.4641e+02
Parnaiba	1.5830e-01	1.4802e-01	2.3373e+01	2.3767e+02
Rhine	1.1835e-01	1.0812e-01	2.9796e+02	8.2340e+02
Rhone	1.5864e-01	1.5453e-01	6.2377e+01	1.6004e+02
Rio grande	2.7069e-01	2.6211e-01	1.3906e+01	1.6057e+02
Saskatchewan	3.4716e-02	8.6115e-02	1.2882e+02	1.8509e+02
Yukon	5.6414e-02	7.2088e-02	4.7868e+02	2.1660e+03
Zambezi	2.4207e-01	2.3779e-01	2.9039e+02	1.1080e+03

Table 2

6.c MEPP results for mean flows

Starting with the lowest MAB, from left to right and top to bottom.

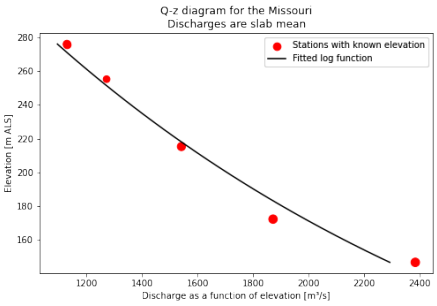

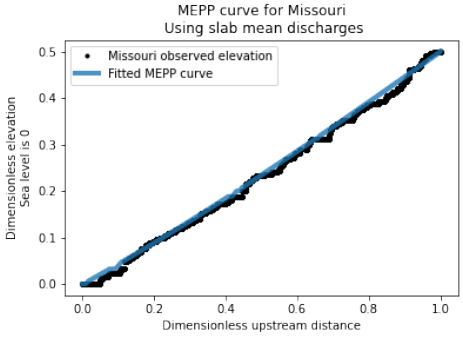

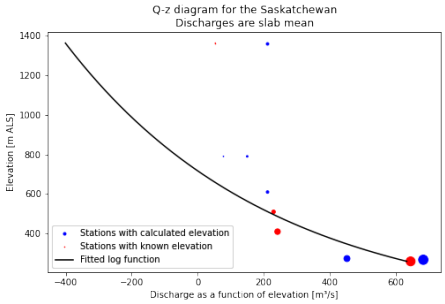

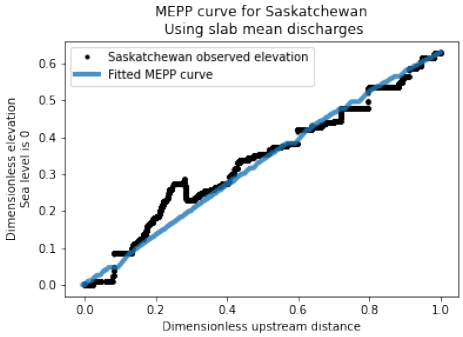

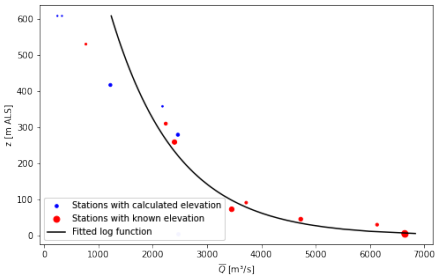

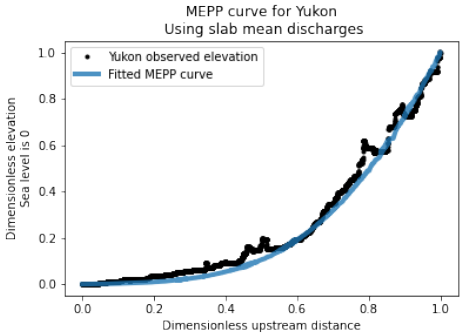

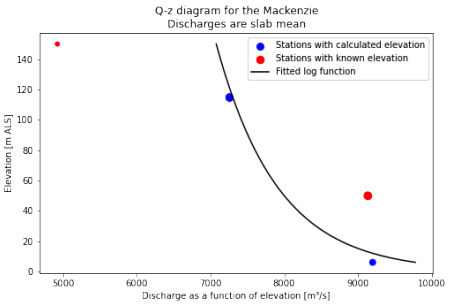

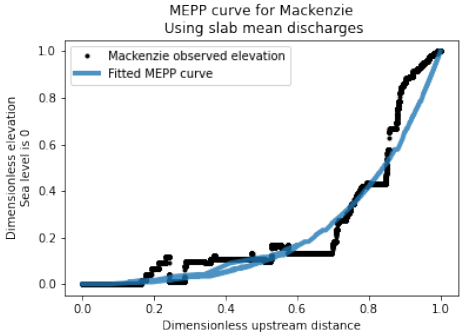

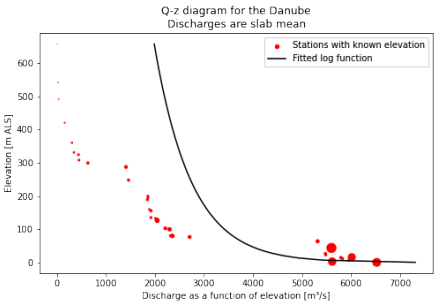
Q-z diagram for the Danube
Discharges are slab mean
Stations with known elevation
Fitted log function
Elevation [m ALS]
Discharge as a function of elevation [m³/s]

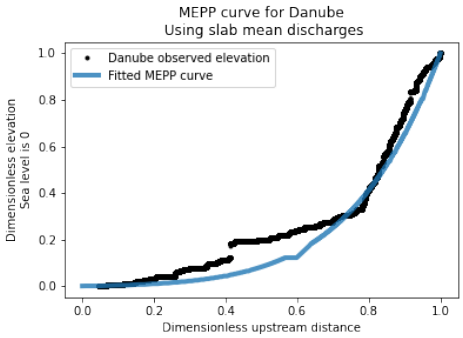
MEPP curve for Danube
Using slab mean discharges
Danube observed elevation
Fitted MEPP curve
Dimensionless elevation
Sea level is 0
Dimensionless upstream distance

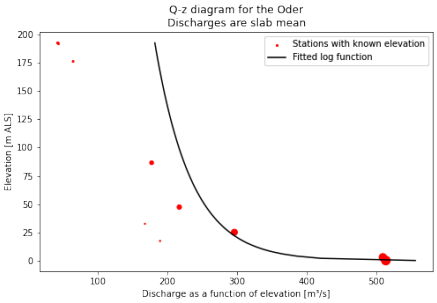
Q-z diagram for the Oder
Discharges are slab mean
Stations with known elevation
Fitted log function
Elevation [m ALS]
Discharge as a function of elevation [m³/s]

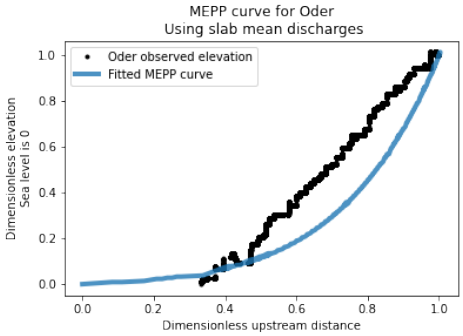
MEPP curve for Oder
Using slab mean discharges
Oder observed elevation
Fitted MEPP curve
Dimensionless elevation
Sea level is 0
Dimensionless upstream distance

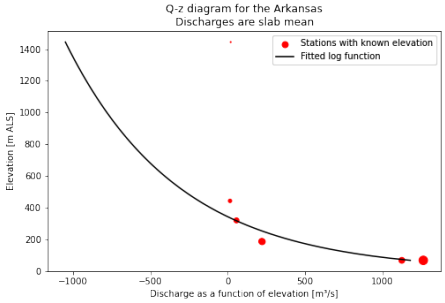
Q-z diagram for the Arkansas
Discharges are slab mean
Stations with known elevation
Fitted log function
Elevation [m ALS]
Discharge as a function of elevation [m³/s]

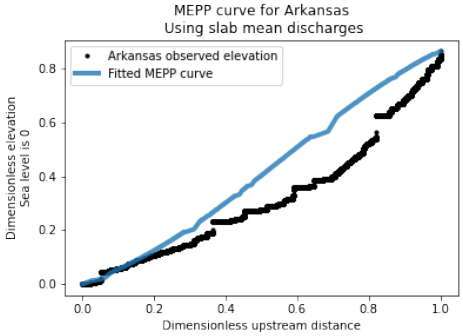
MEPP curve for Arkansas
Using slab mean discharges
Arkansas observed elevation
Fitted MEPP curve
Dimensionless elevation
Sea level is 0
Dimensionless upstream distance

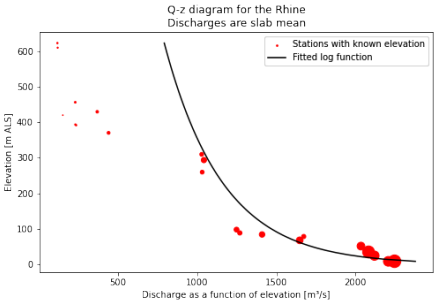
Q-z diagram for the Rhine
Discharges are slab mean
Stations with known elevation
Fitted log function
Elevation [m ALS]
Discharge as a function of elevation [m³/s]

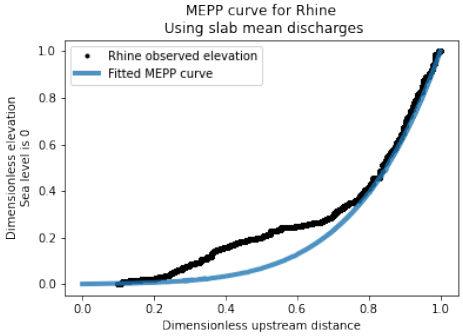
MEPP curve for Rhine
Using slab mean discharges
Rhine observed elevation
Fitted MEPP curve
Dimensionless elevation
Sea level is 0
Dimensionless upstream distance

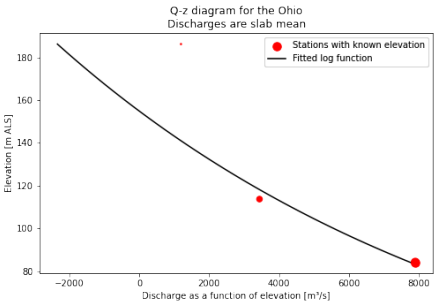
Q-z diagram for the Ohio
Discharges are slab mean
Stations with known elevation
Fitted log function
Elevation [m ALS]
Discharge as a function of elevation [m³/s]

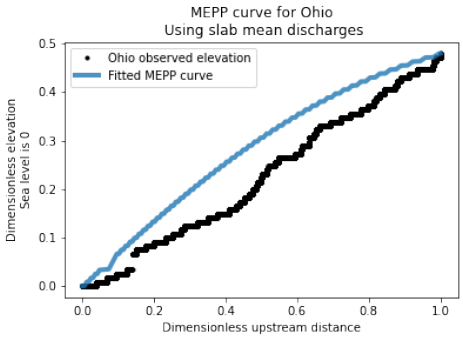
MEPP curve for Ohio
Using slab mean discharges
Ohio observed elevation
Fitted MEPP curve
Dimensionless elevation
Sea level is 0
Dimensionless upstream distance

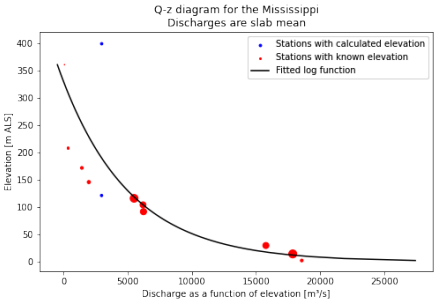
Q-z diagram for the Mississippi
Discharges are slab mean
Stations with calculated elevation
Stations with known elevation
Fitted log function
Elevation [m ALS]
Discharge as a function of elevation [m³/s]

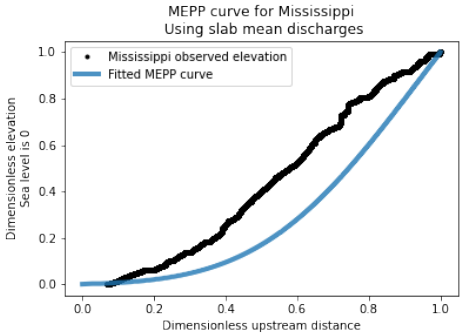
MEPP curve for Mississippi
Using slab mean discharges
Mississippi observed elevation
Fitted MEPP curve
Dimensionless elevation
Sea level is 0
Dimensionless upstream distance

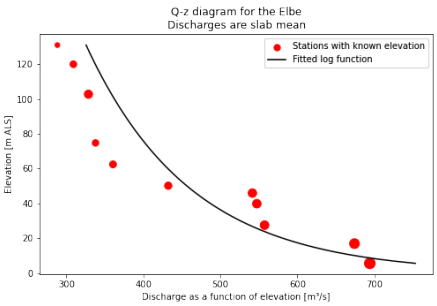
Q-z diagram for the Elbe
Discharges are slab mean
Stations with known elevation
Fitted log function
Elevation [m ALS]
Discharge as a function of elevation [m³/s]

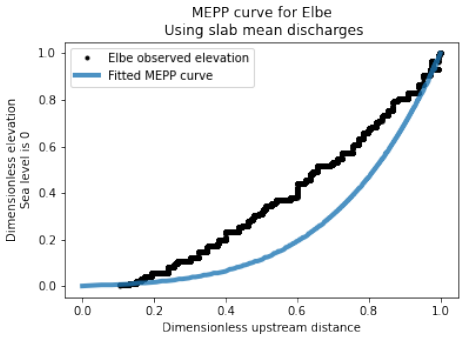
MEPP curve for Elbe
Using slab mean discharges
Elbe observed elevation
Fitted MEPP curve
Dimensionless elevation
Sea level is 0
Dimensionless upstream distance

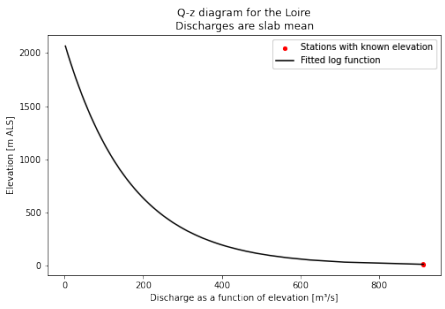
Q-z diagram for the Loire
Discharges are slab mean
Stations with known elevation
Fitted log function
Elevation [m ALS]
Discharge as a function of elevation [m³/s]

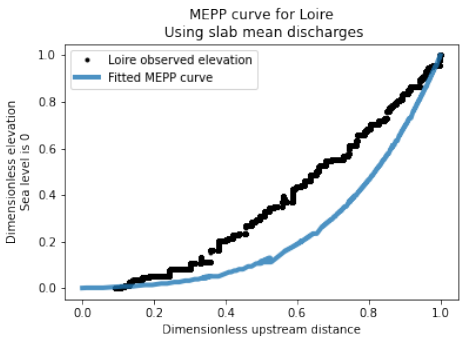
MEPP curve for Loire
Using slab mean discharges
Loire observed elevation
Fitted MEPP curve
Dimensionless elevation
Sea level is 0
Dimensionless upstream distance

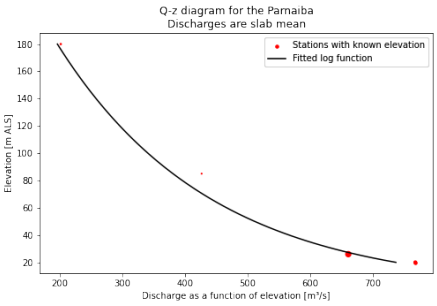
Q-z diagram for the Parnaiba
Discharges are slab mean
Stations with known elevation
Fitted log function
Elevation [m ALS]
Discharge as a function of elevation [m³/s]

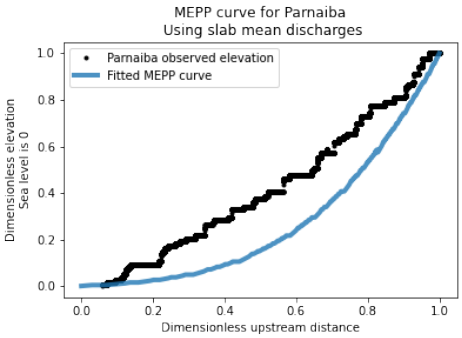
MEPP curve for Parnaiba
Using slab mean discharges
Parnaiba observed elevation
Fitted MEPP curve
Dimensionless elevation
Sea level is 0
Dimensionless upstream distance

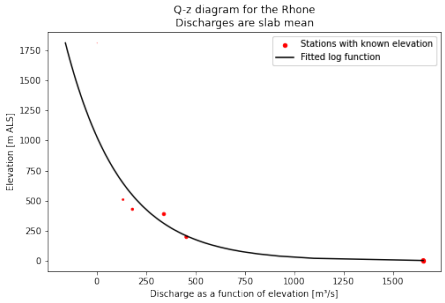
Q-z diagram for the Rhone
Discharges are slab mean
Stations with known elevation
Fitted log function
Elevation [m ALS]
Discharge as a function of elevation [m³/s]

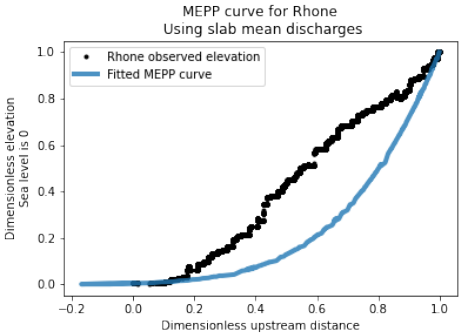
MEPP curve for Rhone
Using slab mean discharges
Rhone observed elevation
Fitted MEPP curve
Dimensionless elevation
Sea level is 0
Dimensionless upstream distance

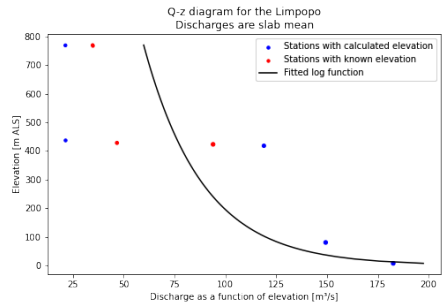
Q-z diagram for the Limpopo
Discharges are slab mean
Stations with calculated elevation
Stations with known elevation
Fitted log function
Elevation [m ALS]
Discharge as a function of elevation [m³/s]

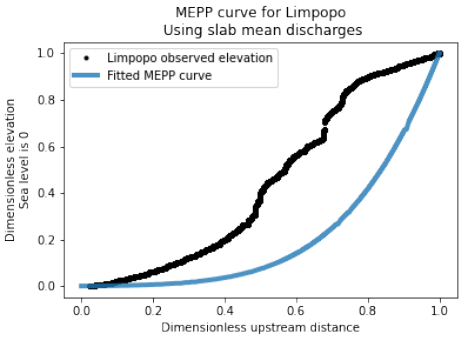
MEPP curve for Limpopo
Using slab mean discharges
Limpopo observed elevation
Fitted MEPP curve
Dimensionless elevation
Sea level is 0
Dimensionless upstream distance

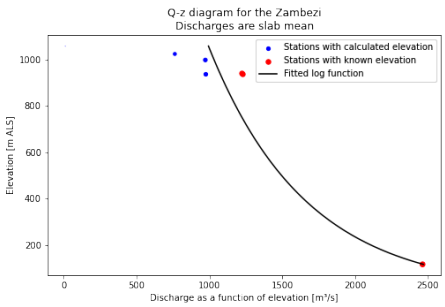
Q-z diagram for the Zambezi
Discharges are slab mean
Stations with calculated elevation
Stations with known elevation
Fitted log function
Elevation [m ALS]
Discharge as a function of elevation [m³/s]

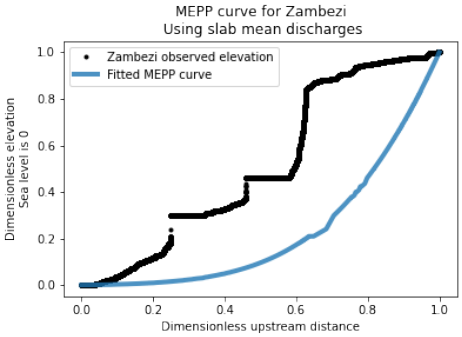
MEPP curve for Zambezi
Using slab mean discharges
Zambezi observed elevation
Fitted MEPP curve
Dimensionless elevation
Sea level is 0
Dimensionless upstream distance

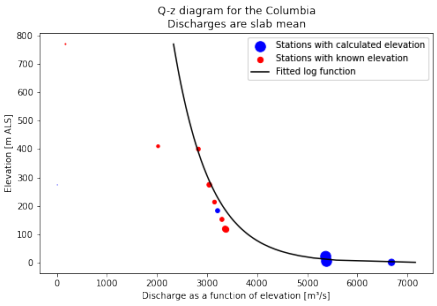
Q-z diagram for the Columbia
Discharges are slab mean
Stations with calculated elevation
Stations with known elevation
Fitted log function
Elevation [m ALS]
Discharge as a function of elevation [m³/s]

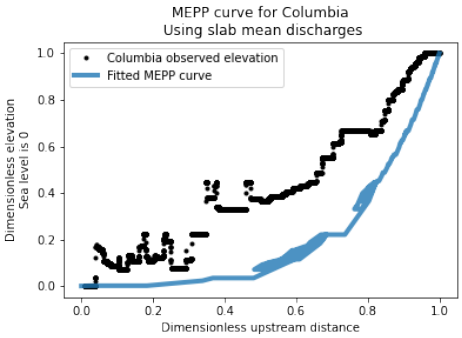
MEPP curve for Columbia
Using slab mean discharges
Columbia observed elevation
Fitted MEPP curve
Dimensionless elevation
Sea level is 0
Dimensionless upstream distance

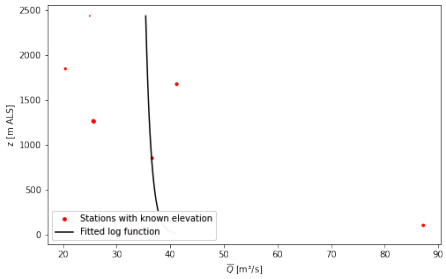
Stations with known elevation
Fitted log function
z [m ALS]
Q [m³/s]

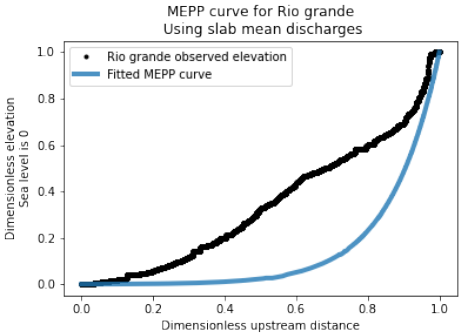
MEPP curve for Rio grande
Using slab mean discharges
Rio grande observed elevation
Fitted MEPP curve
Dimensionless elevation
Sea level is 0
Dimensionless upstream distance

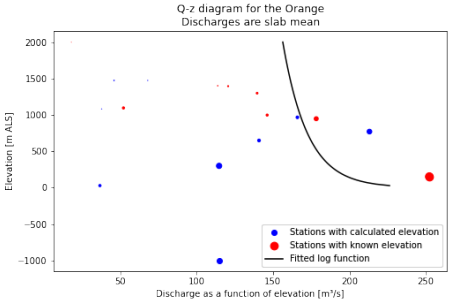
Q-z diagram for the Orange
Discharges are slab mean
Stations with calculated elevation
Stations with known elevation
Fitted log function
Elevation [m ALS]
Discharge as a function of elevation [m³/s]

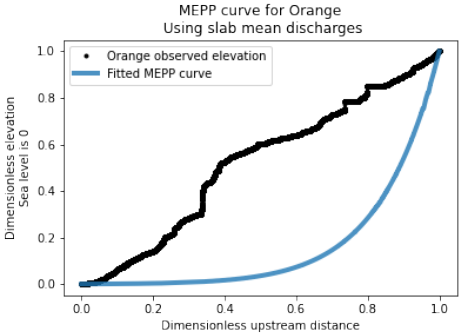
MEPP curve for Orange
Using slab mean discharges
Orange observed elevation
Fitted MEPP curve
Dimensionless elevation
Sea level is 0
Dimensionless upstream distance

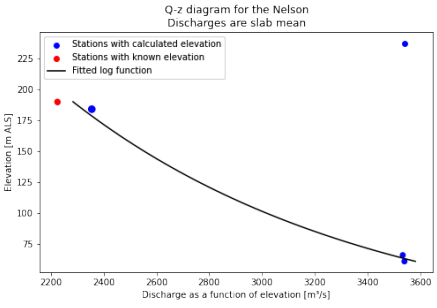
Q-z diagram for the Nelson
Discharges are slab mean
Stations with calculated elevation
Stations with known elevation
Fitted log function
Elevation [m ALS]
Discharge as a function of elevation [m³/s]

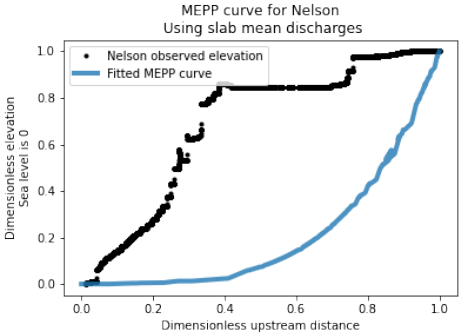
MEPP curve for Nelson
Using slab mean discharges
Nelson observed elevation
Fitted MEPP curve
Dimensionless elevation
Sea level is 0
Dimensionless upstream distance

6.d MEPP results for peak annual flows

Starting with the lowest mean flow MAB, from left to right and top to bottom.

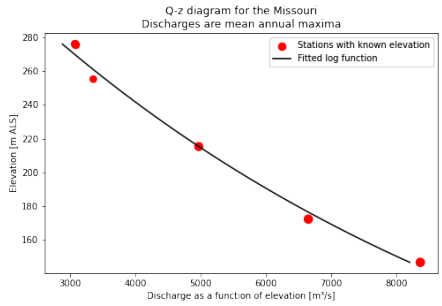

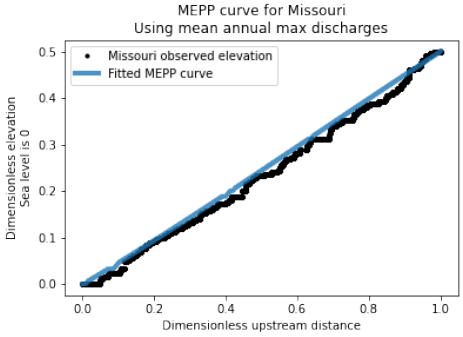

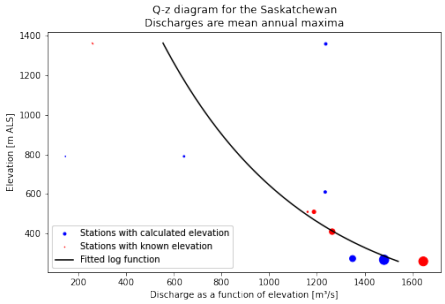

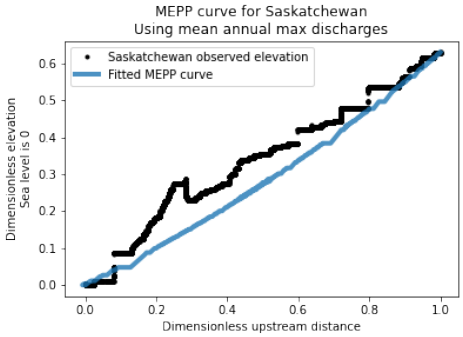

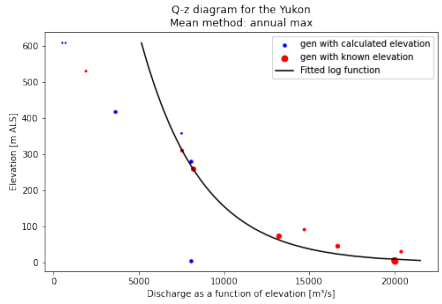

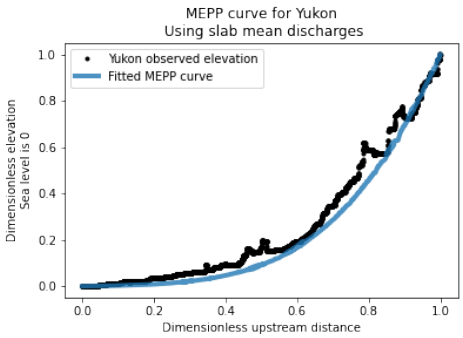

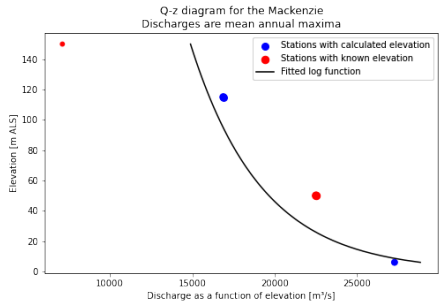

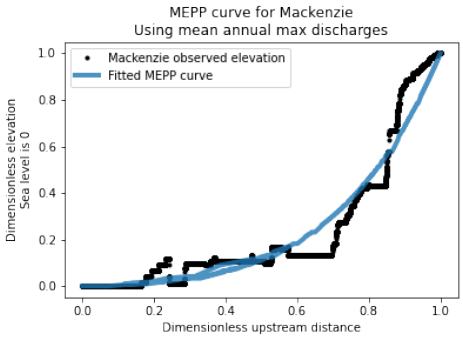

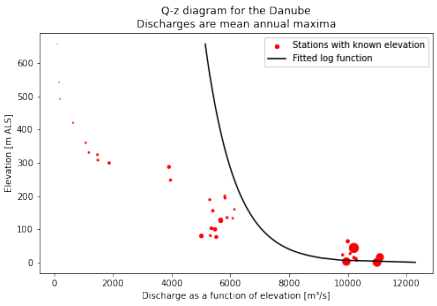
Q-z diagram for the Danube
Discharges are mean annual maxima
Stations with known elevation
Fitted log function
Elevation [m ALS]
Discharge as a function of elevation [m³/s]

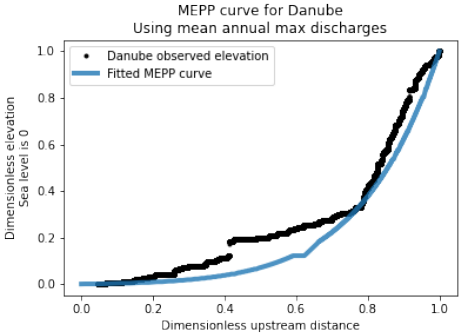
MEPP curve for Danube
Using mean annual max discharges
Danube observed elevation
Fitted MEPP curve
Dimensionless elevation
Sea level is 0
Dimensionless upstream distance

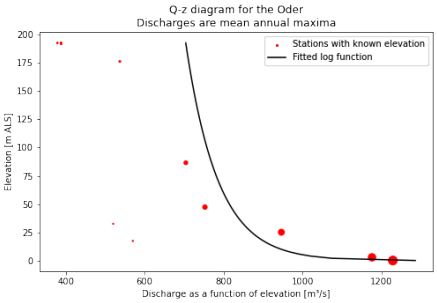
Q-z diagram for the Oder
Discharges are mean annual maxima
Stations with known elevation
Fitted log function
Elevation [m ALS]
Discharge as a function of elevation [m³/s]

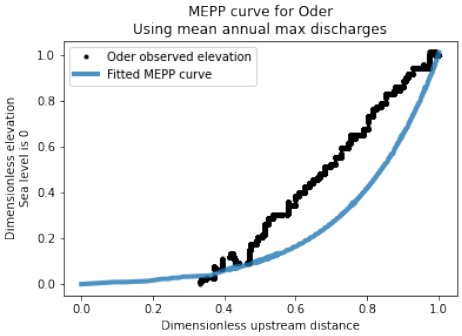
MEPP curve for Oder
Using mean annual max discharges
Oder observed elevation
Fitted MEPP curve
Dimensionless elevation
Sea level is 0
Dimensionless upstream distance

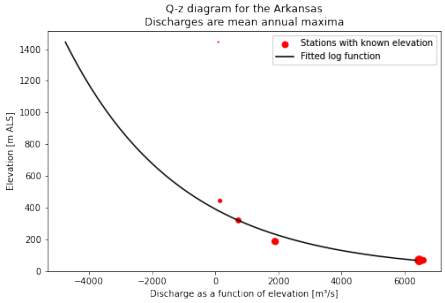
Q-z diagram for the Arkansas
Discharges are mean annual maxima
Stations with known elevation
Fitted log function
Elevation [m ALS]
Discharge as a function of elevation [m³/s]

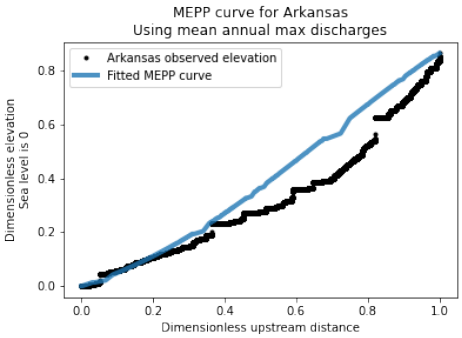
MEPP curve for Arkansas
Using mean annual max discharges
Arkansas observed elevation
Fitted MEPP curve
Dimensionless elevation
Sea level is 0
Dimensionless upstream distance

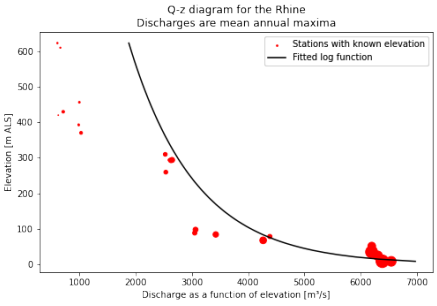
Q-z diagram for the Rhine
Discharges are mean annual maxima
Stations with known elevation
Fitted log function
Elevation [m ALS]
Discharge as a function of elevation [m³/s]

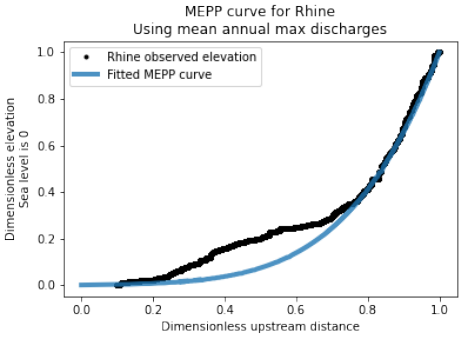
MEPP curve for Rhine
Using mean annual max discharges
Rhine observed elevation
Fitted MEPP curve
Dimensionless elevation
Sea level is 0
Dimensionless upstream distance

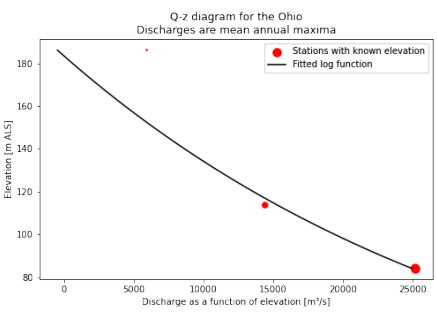
Q-z diagram for the Ohio
Discharges are mean annual maxima
Stations with known elevation
Fitted log function
Elevation [m ALS]
Discharge as a function of elevation [m³/s]

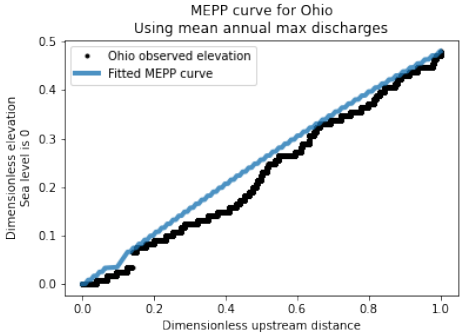
MEPP curve for Ohio
Using mean annual max discharges
Ohio observed elevation
Fitted MEPP curve
Dimensionless elevation
Sea level is 0
Dimensionless upstream distance

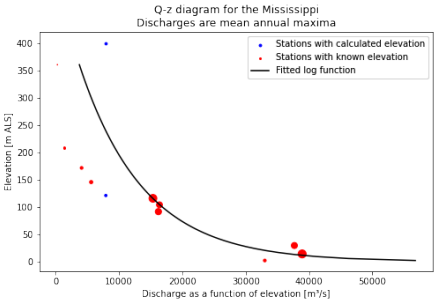
Q-z diagram for the Mississippi
Discharges are mean annual maxima
Stations with calculated elevation
Stations with known elevation
Fitted log function
Elevation [m ALS]
Discharge as a function of elevation [m³/s]

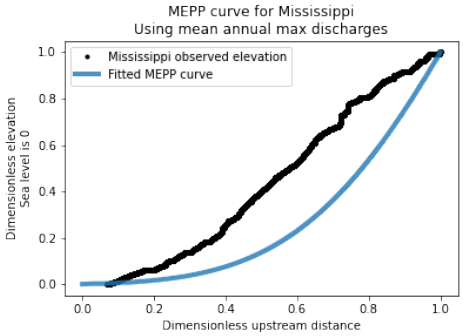
MEPP curve for Mississippi
Using mean annual max discharges
Mississippi observed elevation
Fitted MEPP curve
Dimensionless elevation
Sea level is 0
Dimensionless upstream distance

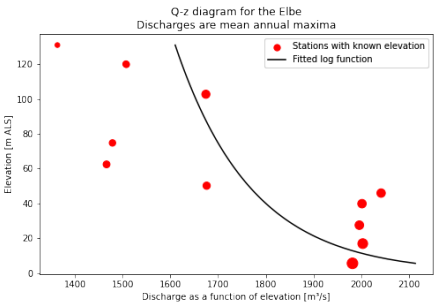
Q-z diagram for the Elbe
Discharges are mean annual maxima
Stations with known elevation
Fitted log function
Elevation [m ALS]
Discharge as a function of elevation [m³/s]

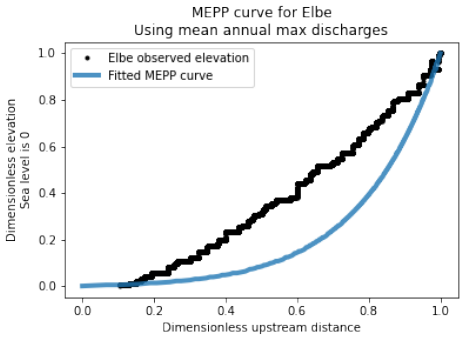
MEPP curve for Elbe
Using mean annual max discharges
Elbe observed elevation
Fitted MEPP curve
Dimensionless elevation
Sea level is 0
Dimensionless upstream distance

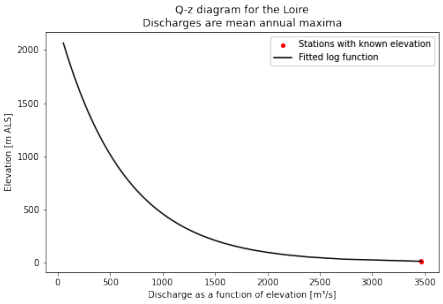
Q-z diagram for the Loire
Discharges are mean annual maxima
Stations with known elevation
Fitted log function
Elevation [m ALS]
Discharge as a function of elevation [m³/s]

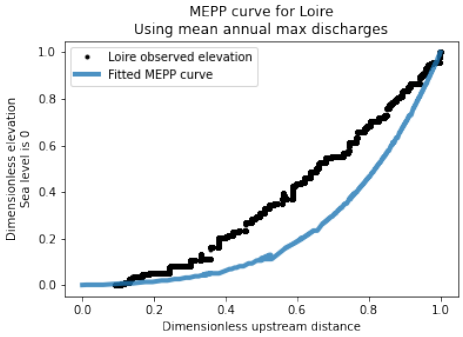
MEPP curve for Loire
Using mean annual max discharges
Loire observed elevation
Fitted MEPP curve
Dimensionless elevation
Sea level is 0
Dimensionless upstream distance

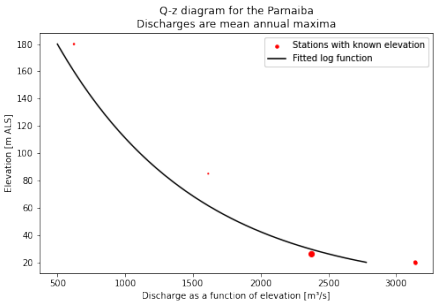
Q-z diagram for the Parnaiba
Discharges are mean annual maxima
Stations with known elevation
Fitted log function
Elevation [m ALS]
Discharge as a function of elevation [m³/s]

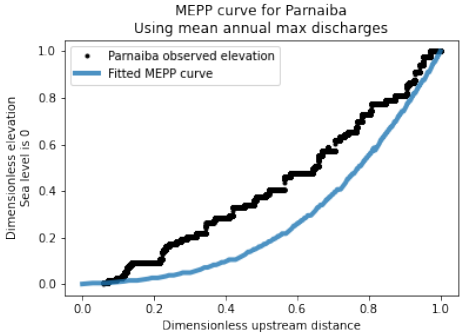
MEPP curve for Parnaiba
Using mean annual max discharges
Parnaiba observed elevation
Fitted MEPP curve
Dimensionless elevation
Sea level is 0
Dimensionless upstream distance

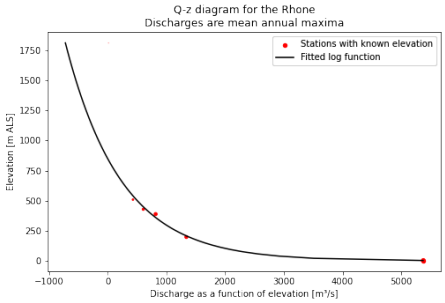
Q-z diagram for the Rhone
Discharges are mean annual maxima
Stations with known elevation
Fitted log function
Elevation [m ALS]
Discharge as a function of elevation [m³/s]

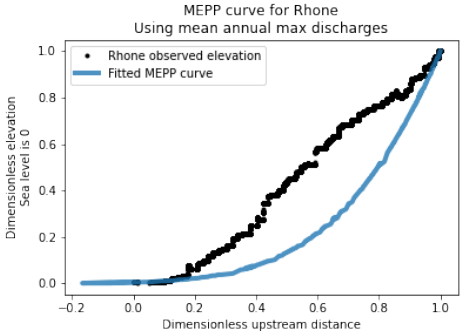
MEPP curve for Rhone
Using mean annual max discharges
Rhone observed elevation
Fitted MEPP curve
Dimensionless elevation
Sea level is 0
Dimensionless upstream distance

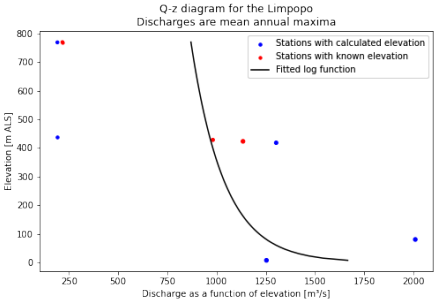
Q-z diagram for the Limpopo
Discharges are mean annual maxima
Stations with calculated elevation
Stations with known elevation
Fitted log function
Elevation [m ALS]
Discharge as a function of elevation [m³/s]

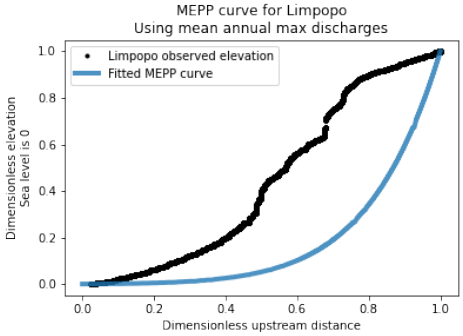
MEPP curve for Limpopo
Using mean annual max discharges
Limpopo observed elevation
Fitted MEPP curve
Dimensionless elevation
Sea level is 0
Dimensionless upstream distance

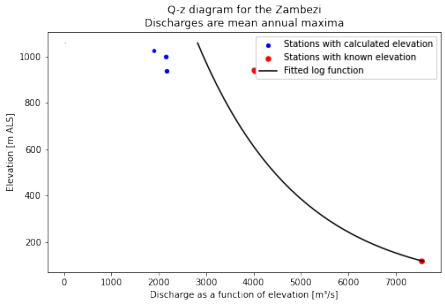
Q-z diagram for the Zambezi
Discharges are mean annual maxima
Stations with calculated elevation
Stations with known elevation
Fitted log function
Elevation [m ALS]
Discharge as a function of elevation [m³/s]

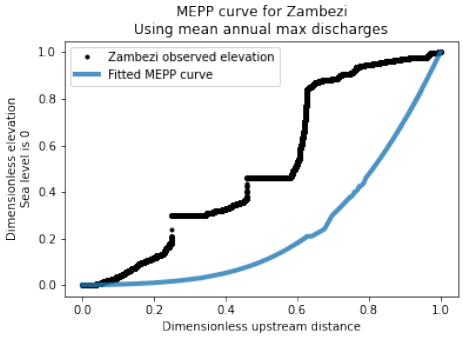
MEPP curve for Zambezi
Using mean annual max discharges
Zambezi observed elevation
Fitted MEPP curve
Dimensionless elevation
Sea level is 0
Dimensionless upstream distance

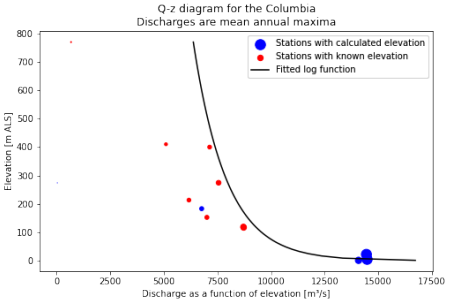
Q-z diagram for the Columbia
Discharges are mean annual maxima
Stations with calculated elevation
Stations with known elevation
Fitted log function
Elevation [m ALS]
Discharge as a function of elevation [m³/s]

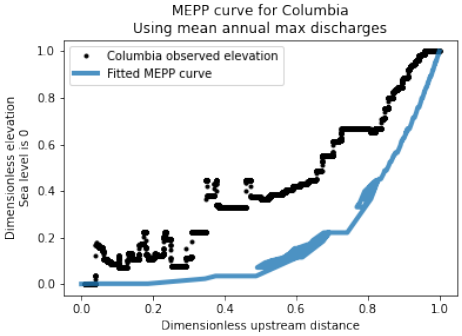
MEPP curve for Columbia
Using mean annual max discharges
Columbia observed elevation
Fitted MEPP curve
Dimensionless elevation
Sea level is 0
Dimensionless upstream distance

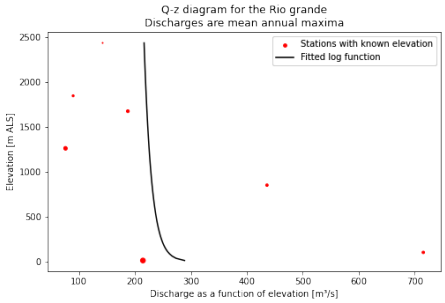
Q-z diagram for the Rio grande
Discharges are mean annual maxima
Stations with known elevation
Fitted log function
Elevation [m ALS]
Discharge as a function of elevation [m³/s]

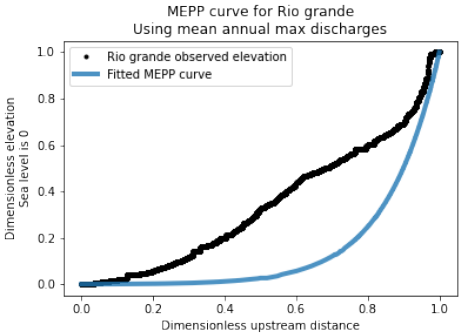
MEPP curve for Rio grande
Using mean annual max discharges
Rio grande observed elevation
Fitted MEPP curve
Dimensionless elevation
Sea level is 0
Dimensionless upstream distance

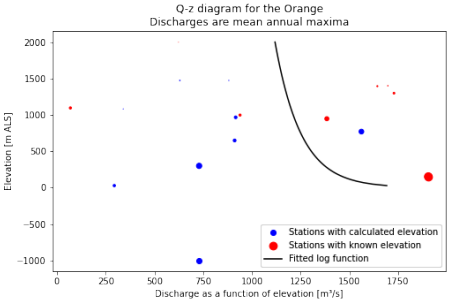
Q-z diagram for the Orange
Discharges are mean annual maxima
Stations with calculated elevation
Stations with known elevation
Fitted log function
Elevation [m ALS]
Discharge as a function of elevation [m³/s]

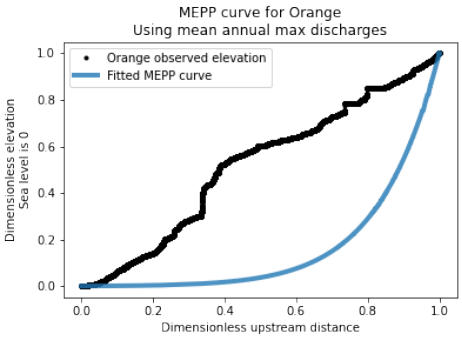
MEPP curve for Orange
Using mean annual max discharges
Orange observed elevation
Fitted MEPP curve
Dimensionless elevation
Sea level is 0
Dimensionless upstream distance

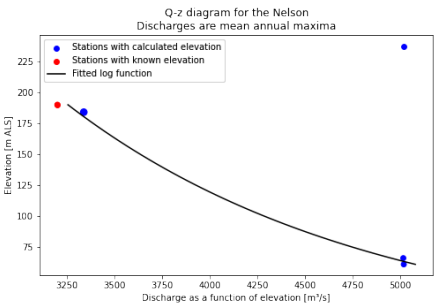
Q-z diagram for the Nelson
Discharges are mean annual maxima
Stations with calculated elevation
Stations with known elevation
Fitted log function
Elevation [m ALS]
Discharge as a function of elevation [m³/s]

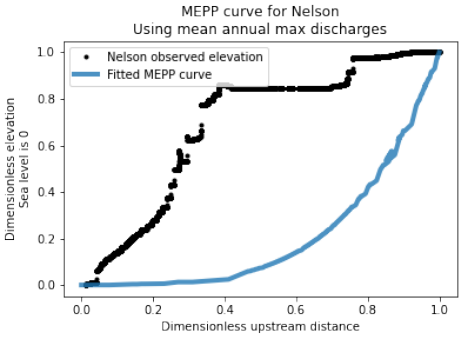
MEPP curve for Nelson
Using mean annual max discharges
Nelson observed elevation
Fitted MEPP curve
Dimensionless elevation
Sea level is 0
Dimensionless upstream distance

References

Bertoldi, W. (2010). Assessment of morphological changes induced by flow and flood pulses in a gravel bed braided river: The Tagliamento River (Italy). *Geomorphology*, 114(3):348.

Chang, H. H. (2008). River morphology and river channel changes. *Transactions of Tianjin University*, 14:254–262.

Faraoni, V. (2020). Maximizing friction in the erosion of glacial valleys. *Journal of Glaciology*, 66:876–879.

Garrick, D. E. (2018). Decentralisation and drought adaptation: applying the subsidiarity principle in transboundary river basins. *International Journal of the Commons*, 12(I):301–331.

Hirano, M. and Aniya, M. (1988). A rational explanation of cross-profile morphology for glacial valleys and of glacial valley development. *Earth Surface Processes and Landforms*, 13:707–716.

Jenkins, S. A. and Inman, D. L. (2006). Thermodynamic solutions for equilibrium beach profiles. *Journal of Geophysical Research*, 111:C02003.

Kleidon, A. (2020). Understanding the Earth as a whole system: From the Gaia Hypothesis to Thermodynamic Optimality and Human Societies. In Schlaudt, O. and König, P., editors, *Was ist Kosmos? Im Dialog der Disziplinen*. Heidelberg University Press.

Kleidon, A., Fraedrich, K., Kirk, E., and Lunkeit, F. (2006). Maximum entropy production and the strength of boundary layer exchange in an atmospheric general circulation model. *Geophysical Research Letters*, 33(6).

Kleidon, A., Yadvinder, M., and Cox, P. M. (2010). Maximum entropy production in environmental and ecological systems. *Phil. Trans. R. Soc. B*, 365:1297–1302.

Koutsoyiannis, D. (2014). Entropy: From thermodynamics to hydrology. *Entropy*, 16(3):1287–1314.

Lehner, B., Verdin, K., and Jarvis, A. (2008). New global hydrography derived from spaceborne elevation data. *Eos, Transactions, AGU*, 89(10):93–94.

Looser, U., Faerber, C., Recknagel, T., and Plessow, H. (2020). The Global Runoff Data Centre, 56068 Koblenz, Germany.

Maheu, A., Hajji, I., Anctil, F., Nadeau, D. F., and Therrien, R. (2019). Using the maximum entropy production approach to integrate energy budget modelling in a hydrological model. *Hydrology and Earth System Sciences*, 23(9):3843–3863.

Maldonado, S. and Uchasara, M. (2019). On the thermodynamics-based equilibrium beach profile derived by Jenkins and Inman. *arXiv: Geophysics*.

Martyushev, L. and Seleznev, V. (2013). Maximum entropy production principle (MEPP). Comment about restrictions and typical misconceptions of critics of MEPP.

Morgan, F. (2005). A note on cross-profile morphology for glacialvalleys. *Earth Surface Processes and Landforms*, 30:513–514.

Osterkamp, W., Lane, L., and Foster, G. (1983). An analytical treatment of channel-morphology relations. Technical report, US Geological Survey, Washington.

Porada, P., Kleidon, A., and Schymanski, S. J. (2011). Entropy production of soil hydrological processes and its maximisation. *Earth System Dynamics*, 2(2):179–190.

Porter, Claire, e. a. (2018). Arctic Dem.

Saville, C. (2013). *Fluvial and tectonic geomorphology of orogenic plateaux*. PhD thesis, Durham University.

Swenson, R. (1997). Autocatakinetics, evolution and the law of Maximum Entropy Production: A principled foundation towards the study of human ecology. *Advanced Human Ecology*, 6:1–47.

USGS (1996). Global 30 Arc-Second Elevation (GTOPO30).

Warmink, J., Booij, M., H, K., and Hulscher, S. (2007). Uncertainty in water level predictions due to various calibrations. *Proceedings International Conference on Adaptive and Integrative Water Management (CAIWA)*, page 18 pages.

Westhoff, M. C. and Zehe, E. (2013). Maximum entropy production: can it be used to constrain conceptual hydrological models? *Hydrological Earth System Sciences*, 17:3141–3157.

Yatsu, E. (1955). On the longitudinal profile of the graded river. *Eos, Transactions American Geophysical Union*, 36(4):655–663.

Ylla Arbós, C., Blom, A., Viparelli, E., Reneerkens, M., Frings, R. M., and Schielen, R. M. J. (2021). River response to anthropogenic modification: Channel steepening and gravel front fading in an incising river. *Geophysical Research Letters*, 48(4):e2020GL091338.

Zhao, J., Wang, D., Yang, H., and Sivapalan, M. (2016). Unifying catchment water balance models for different time scales through the maximum entropy production principle. *Water Resources Research*, 52(9):7503–7512.